Rapid Communications in Mass Spectrometry
October 2020, Volume 34, Issue 19, Pages e8859 (12p.)
https://doi.org/10.1002/rcm.8859
https://archimer.ifremer.fr/doc/00633/74524/

Characterization of maitotoxin- 4 (MTX4) using electrospray positive mode ionization high- resolution mass spectrometry and UV spectroscopy

Pisapia Francesco [1], Sibat Manoella [1], Watanabe Ryuichi [2], Roullier Catherine [3], Suzuki Toshiyuki [2], Hess Philipp [1, *], Herrenknecht Christine [3]

[1] Ifremer, DYNECO Rue de l'Île d'Yeu 44311 Nantes, France
[2] NRIFS, Japan Fisheries Research and Education Agency 2-12-4 Fukuura, Kanazawa-ku Yokohama Kanagawa 236-8648, Japan
[3] Université de Nantes, MMS EA2160, Faculté de Pharmacie 9 rue Bias 44035 Nantes, France

* Corresponding author : Philipp Hess, email address : philipp.hess@ifremer.fr

Abstract :

Rationale

The dinoflagellate genera Gambierdiscus and Fukuyoa are producers of toxins responsible for Ciguatera Poisoning (CP). Although having very low oral potency, maitotoxins (MTXs) are very toxic following intraperitoneal injection and feeding studies have shown they may accumulate in fish muscle. To date, six MTX congeners have been described but two congeners (MTX2 and MTX4) have not yet been structurally elucidated. The aim of the present study was to further characterize MTX4.

Methods

Chemical analysis was performed using Liquid Chromatography coupled to a Diode Array Detector (DAD) and positive ionization mode High Resolution Mass Spectrometry (LC/HRMS) on partially purified extracts of G. excentricus (strain VGO792). HRMS/MS studies were also carried out to tentatively explain the fragmentation pathways of MTX and MTX4.

Results

The comparison of UV and HRMS (ESI+) spectra between MTX and MTX4 led us to propose the elemental formula of MTX4 (C157H241NO68S2, as unsalted molecule). The comparison of the theoretical and measured m/z values of the doubly charged ions of the isotopic profile in ESI+ were coherent with the proposed elemental formula of MTX4. The study of HRMS/MS spectra on the tri-ammoniated adduct ([M–H+3NH4]2+) of both molecules gave additional information about structural features. The cleavage observed, probably located at C99–C100 in both MTX and MTX4, highlighted the same A-side product ion shared by the two molecules.
Conclusion

All these investigations on the characterization of MTX4 contribute to highlighting that MTX4 belongs to the same structural family of MTXs. However to accomplish a complete structural elucidation of MTX4, NMR-based study and LC/HRMSn investigation will have to be carried out.

INTRODUCTION

The epi-benthic dinoflagellate genera *Gambierdiscus* and *Fukuyoa* are the primary producers of the toxins responsible for Ciguatera Poisoning (CP), the most common non-bacterial food poisoning, mostly due to consumption of fish [1–3].

Recent studies revealed that *G. excentricus* is one of the most toxic species known to date, for production of both ciguatoxins (CTXs) and maitotoxins (MTXs) [3–7]. Ciguatoxins (CTXs) are the main known causative agents of CP [8]. Although having very low oral potency [7,9], maitotoxins (MTXs) are very toxic following intraperitoneal injection [10] and feeding studies by Kohli et al [11] in laboratory-controlled conditions have shown they may accumulate in fish muscle. To date, six MTX congeners have been described: maitotoxin (MTX) [10,12–14], maitotoxin-2 (MTX2) [15], maitotoxin-3 (MTX3) [16] and maitotoxin-4 (MTX4) [17], as well as two further mono-sulfated analogues of MTX [18]. Maitotoxin (MTX) is the largest non-polymeric marine toxin identified to date, consisting of a ladder-shaped cyclic polyether that is composed of 32 fused ether rings, 28 hydroxyl groups, 21 methyl groups, two sulfates and 98 chiral centers (elemental formula: $C_{164}H_{256}O_{68}S_2Na_2$, accurate mono-isotopic mass of 3423.5811 Da for the di-sodium salt) (**Figure 1**) [10,19,20].

Since the most recent taxonomic separation into species and phylotypes, production of MTX has solely been confirmed in strains of *G. australes* [17,21–24]. The first description of MTX3 dates back to 1994 [16]. Since then, LC/MS/MS analyses revealed the presence of putative MTX3 in several *Gambierdiscus* and *Fukuyoa* species [17,21–37]. The molecular structure of this compound was recently elucidated in two concurrent articles, after isolation from both *G. australes* [38] and *G. belizeanus* [39]. Both articles agree with MTX3 actually being 44-methylgambierone, a congener of gambierone, another sulfated polyether compound that has recently been isolated from *G. belizeanus* [40]. Since the recent structural description of 44-methylgambierone, it has also been detected in other *Gambierdiscus* species [41,42].

Two MTX congeners (MTX2 and MTX4) have not yet been structurally elucidated [15–17,43]. The recent investigation of MTX4 (accurate mono-isotopic mass of 3292.4860 Da for the free acid form) included neuro-2a cytotoxicity data and high resolution mass spectrometry (HRMS) analysis in negative electrospray ionization mode (ESI^-) and suggested that this toxin is specific to *G. excentricus* [17].

The previous HRMS/MS (ESI^-) experiments on MTX and MTX4 were not very informative, as they only resulted in the loss of sulfate group(s) [17]. The aim of the present study was to make a step further into the chemical characterization of MTX4. In order to achieve this goal, chemical analyses were performed using a UHPLC system coupled to a diode array detector

(DAD) and a Q-Tof 6550 iFunnel high resolution mass spectrometer (Agilent Technologies, Santa Clara, CA, USA) operating in positive electrospray ionization mode (ESI^+).

Comparison of UV, HRMS (ESI^+) and HRMS/MS (ESI^+) spectra brought to light new similarities and differences between MTX and MTX4. The elemental formula of MTX4 was proposed and additional information was gained about its structural features.

EXPERIMENTAL

Chemicals and Reagents

Maitotoxin (MTX) was purchased from Wako Chemicals GmbH (Neuss, Germany) and was used as reference standard for DAD and mass spectral analyses. MTX was dissolved and stored in MeOH:H_2O (1:1, v/v). The stock solution was prepared at a concentration of 50 µg mL^{-1}.

HPLC-grade methanol was purchased from Sigma Aldrich (Saint Quentin Fallavier, France). Milli-Q water was supplied by a Milli-Q integral 3 system (Millipore, Saint-Quentin-Yvelines, France). High purity water (Optima LC-MS quality), acetonitrile (Optima LC-MS quality), formic acid (Puriss quality) and ammonium formate (Purity for MS) were used to prepare mobile phases; they were purchased from Fisher Scientific (Illkirch, France).

Sample Preparation

Cell pellets were collected from *Gambierdiscus excentricus* culture (strain VGO792, Punta Hidalgo, Tenerife, Canary Islands, Spain). Full details description on culture conditions, extraction and purification steps can be found in Pisapia et al [17]. The most concentrated toxic fractions of *G. excentricus* extracts containing maitotoxin-4 (MTX4) were used for this study.

Liquid chromatography-high resolution mass spectrometry (Q-Tof 6550 iFunnel)

Liquid chromatography coupled to high resolution mass spectrometry (LC/HRMS) was performed using a UHPLC system (1290 Infinity II, Agilent Technologies) coupled to a diode array detector (DAD, Agilent Technologies, CA, USA) and to a high resolution time-of-flight mass spectrometer (Q-Tof 6550 iFunnel, Agilent Technologies) equipped with a Dual Jet Stream® electrospray ionization (ESI) interface.

Toxins were separated using a reversed-phase C_{18} Kinetex column (100 Å, 2.6 µm, 50 × 2.1 mm, Phenomenex, Le Pecq, France) with water (A) and 95% acetonitrile/water (B), both containing acidic buffer consisting of formic acid (HCOOH), 50 mM, and ammonium formate ($HCOO^-NH_4^+$), 2 mM. The column oven and the sample tray temperatures were set at 40 °C and 4 °C, respectively. The flow rate was set at 0.4 mL min^{-1}, and the injection volume was set

at 3 µL. Separation was achieved using the following mobile phase gradient: from 10% to 95% B in 10 min, plateau at 95% B for 2 min, return to the initial condition (10% B) in 0.1 min and a re-equilibration period (10% B) for 3.9 minutes. The chromatographic run lasted 16 min per analysis. The MTX standard used for LC/HRMS experiments was at a concentration of 20 µg mL^{-1} MeOH:H_2O (1:1, v/v).

The diode array detector (Agilent Technologies) was set to acquire spectra in a range of wavelengths between 200 and 400 nm, every 2 nm. The extracted signal for MTX and MTX4 was chosen as follows: 260 ± 30 nm. UV spectra of a blank sample, consisting of MeOH:H_2O (1:1, v/v) injected under the same analytical conditions, were subtracted from MTX and MTX4 spectra. The conditions of the ESI^+ source were set as follows: source temperature, 200 °C; drying gas, N_2; flow rate, 11 mL min^{-1}; sheath gas temperature, 350 °C; sheath gas flow rate, 11 mL min^{-1}; nebulizer, 45 psig; capillary voltage, 3.5 kV; nozzle voltage, 500 V. The instrument was mass calibrated in positive ionization mode before each analysis, using the Agilent tuning mix. A mixture solution of reference mass compounds (purine, 2 mL L^{-1}; HP-0921, 1 mL L^{-1}; HP-1221, 1 mL L^{-1}; HP-1821, 2 mL L^{-1}; HP-2421, 2 mL L^{-1}) in MeOH:H_2O (95:5, v/v) was infused with an isocratic pump to a separate ESI sprayer in the dual spray source at a constant flow rate of 1.5 µL min^{-1}. HP-0921 and purine allowed for correction of the measured *m/z* values throughout the batch. Mass spectral detection was carried out in full scan and targeted MS/MS mode in positive ion mode. The full scan acquisition operated at a mass resolution of 45,000 Full Width at Half Maximum (FWHM) over a *m/z* range from 100 to 3200 with a scan rate of 2 spectra s^{-1}. The targeted MS/MS mode was performed in a Collision Induced Dissociation (CID) cell using a mass resolving power of 45,000 FWHM over the *m/z* range from 40 to 3200 with a MS scan rate of 10 spectra s^{-1} and a MS/MS scan rate of 3 spectra s^{-1}. Different collision energies (from 10 to 50 eV) were applied to the precursor ions to obtain good fragmentation. All the acquisition and analysis data were controlled by MassHunter software (Agilent Technologies).

Elemental formula modelling of MTX4 using ChemCalc

Isotope ratio modelling and determination of elemental formulae were performed with ChemCalc, an open source software [44]. For each monoisotopic ion (and bi- and tri-charged molecule-related ions acquired in negative and positive ion mode), the measured accurate mass and its charge were entered in the Molecular Formula Finder application, to obtain the most appropriate hypothetical elemental formulae. To increase the relevance of the search, elemental formulae presenting a $|\Delta ppm| < 10$ were pre-selected and other filters were added, such as the

most likely range for the number of carbon, nitrogen, oxygen, hydrogen, sulfur atoms and unsaturations. Subsequently, the theoretical isotopic ratio profiles simulated by ChemCalc were compared with the experimental ones.

RESULTS and DISCUSSION

Retention times

For the present study in positive ion mode, the mobile phases were buffered with formic acid (HCOOH, 50 mM) and ammonium formate ($HCOO^-NH_4^+$, 2 mM). The acidic buffer improved positive ionization of MTXs as it allowed the formation of intense ammonium adducts.

An increase of the retention time (*RT*) of both MTXs was observed compared with the previous study [17]. MTX eluted at 5.74 min (instead of 4.09 min), and MTX4 eluted at 5.56 min (instead of 4.58 min) (**Table 1**). This increase in *RT* can be explained by the presence of the sulfate groups, i.e. anionic functional groups. In aqueous mixtures, sulfated compounds undergo acid-base equilibrium between the acid-form ($R–OSO_3H$) and the deprotonated form ($R–OSO_3^-$). In acidic conditions, a shift of this equilibrium in favor of the acid-form make MTXs less polar, resulting in increased retention on a reversed-phase column. Interestingly, the increase in *RT* was less pronounced in MTX4 (ΔRT = +0.98 min) than in MTX (ΔRT = +1.65 min).

UV spectra

Maitotoxin (MTX) was characterized by a single UV absorbance maximum at 232 nm (**Figure 2B**), slightly higher than what was previously reported by Yokoyama, et al [45] (i.e. λ_{max} = 230 nm). The UV absorption is due to the presence of a conjugated diene function at one extremity of the molecule ($C_2–C_3–C_4–C_{144}$, **Figure 1**).

Maitotoxin-4 (MTX4) exhibited a UV spectrum composed of a UV maximum at 275 nm with two shoulders (**Figure 2D**). The bathochromic effect of +43 nm, compared with MTX, suggests the presence of more conjugated unsaturations or the presence of an amine- (or even amide-) substituent on a conjugated diene function [46]. The presence of an amine function is supported by the earlier elution of MTX4 than of MTX under acidic mobile phase conditions. Indeed, when the pH is decreased the sulfate group is protonated for MTX and MTX4, increasing the lipophilicity of the two molecules, while the amine group is also protonated for MTX4, leading to a decrease in lipophilicity.

Elemental formula determination of MTX4

As previously described [17], MTX4 was assumed to have an accurate calculated mass of 3292.4860 (free acid form) with a bi-charged $[M–2H]^{2–}$ anion at *m/z* 1645.2357 and a tri-charged anion at *m/z* 1096.4889 $[M–3H]^{3–}$. In the same manner, this study found a doubly charged cation at *m/z* 1647.2500 $[M+2H]^{2+}$ in positive HRMS spectra of MTX4 allowing us to confirm: (i) the calculated mass of 3292.4860 for MTX4 and (ii) the difference of 87.13 Da from MTX.

For modelling of the elemental formula of MTX4 in ChemCalc, the following assumptions were made: the molecule had 30 to 45 unsaturations, two sulfur atoms and one to five nitrogen atoms. The assumption of two sulfur atoms derived from the mass spectral evidence described late, i.e. two sulfate losses (**Table 3** and **Figure 4**). The assumption of a similar number of unsaturations in MTX4 and MTX was derived from the similar molecular size of MTX4 to MTX, the substantial similarity in the A-side of the molecule and the bathochromic effect described above (UV spectra), suggesting an increased number of conjugated unsaturations. Therefore, a range from 30 to 45 unsaturations was chosen in ChemCalc. The presence of an uneven number of nitrogen atoms in MTX4 derived from the "nitrogen rule" [47], considering the absence of nitrogen in MTX and the uneven mass difference between MTX and MTX4.

The accurate mono-isotopic *m/z* value of the eight ion species of MTX4 reported in **Table 2** were used for modelling the elemental formula of MTX4 in ChemCalc. The following filters were applied: (i) range of atoms: C100–200 H200–400 N1–5 O50–150 S2, (ii) 30–45 unsaturations and (iii) mass accuracy range of ±10 ppm. The average of the absolute values of Δppm (|Δppm|) was calculated for each of the formulae proposed, taking into account all the eight ion species of MTX4 (**Table S1, supporting information**). A total of 20 raw formulae with an average |Δppm| < 10 were considered as potential candidates for the elemental formula of MTX4 (**Table S1, supporting information**). The first seven formulae with the best ranking score (average |Δppm| < 3, **Table S1, supporting information**) were chosen for further consideration. The experimental isotopic profiles of the most intense ion clusters of th full scan positive and negative ion spectra of MTX4 ($[M-H+3NH_4]^{2+}$, $[M+2NH_4]^{2+}$ and $[M-2H]^{2-}$) were compared with the theoretical ones simulated by ChemCalc for the seven sum formulae. The study of the isotopic profiles did not allow for discrimination between the seven formulae since the relative abundances of isotopic peaks were very similar (**Table S2, supporting information**). Nevertheless, some of the formulae (#02, #03, #05, **Table S1, supporting information**) could be excluded considering that the degrees of unsaturation were either too low (30 for #02) or too high (43 for #03 and #05) compared with MTX (36). Also, the formulae

containing three (#01 and #03, **Table S1, supporting information**) and five (#02, #05 and #06, **Table S1**) nitrogen atoms seem unlikely compared with MTX. Therefore, the elemental formula of MTX4 could be either $C_{157}H_{241}NO_{68}S_2$ (#04, average |Δppm| = 2.3, 38 unsaturations, **Table S1, supporting information**) or $C_{153}H_{241}NO_{71}S_2$ (#07, average |Δppm| = 2.9, 34 unsaturations, **Table S1, supporting information**). Based on the lower average |Δppm|, and further mass spectrometric evidence of positive ion product ions presented below, we propose a formula of $C_{157}H_{241}NO_{68}S_2$ (#04): MTX4 would thus contain one nitrogen atom more than MTX, and seven carbons and 17 hydrogens less than MTX, and presents two additional unsaturations, i.e. MTX4 has 38 unsaturations, and MTX has 36 unsaturations.

Positive electrospray HRMS spectra

Due to the knowledge of the elemental formula of the MTX, the assignment of the most intense positive ion clusters was readily achieved and attributed to the singly, doubly and triply ammoniated adducts at *m/z* 1699.3240, 1707.8323 and 1716.3500, $[M+H+NH_4]^{2+}$, $[M+2NH_4]^{2+}$ and $[M–H+3NH_4]^{2+}$, respectively (**Figure 3A**; **Table 2**). In parallel, the HRMS spectra of MTX4 presented the same ion cluster profile with mono-isotopic ions at *m/z* 1647.2500, 1655.7575, 1664.2725 and 1672.7870, corresponding to $[M+2H]^{2+}$, $[M+H+NH_4]^{2+}$, $[M+2NH_4]^{2+}$ and $[M–H+3NH_4]^{2+}$, respectively. For both MTXs, the mass differences (Δppm) between measured and exact theoretical mass were acceptable (< 7 ppm) for all the mono-isotopic ions (**Table 2**) and also confirmed the elemental formula of MTX4 ($C_{157}H_{241}NO_{68}S_2$).

Differences in intensity ratios between the ion clusters of MTX and MTX4 in positive mode were observed (**Figure 3**). The ion species $[M+2NH_4]^{2+}$ was predominant in the spectrum of MTX (**Figure 3A**), whereas $[M–H+3NH_4]^{2+}$ was the most intense cluster in the case of MTX4 (**Figure 3B**).

Molecule-related ion cluster fragmentation patterns of MTX and MTX4 (losses of water and sulfate)

Fragmentation of the doubly charged molecular anions $[M–2H]^{2–}$ of MTX and MTX4 in negative ESI HRMS/MS mode was provided in a previous study [17]. In both cases, the HRMS/MS spectra were dominated by a single product ion peak corresponding to the hydrogenated sulfate anion ($[HOSO_3]^–$).

In positive ioni mode, it was not possible to target the doubly charged molecular cation $[M+2H]^{2+}$ since its intensity was too weak. Due to its large intensity, the tri-ammoniated adduct ($[M–H+3NH_4]^{2+}$) of MTX4 was chosen for fragmentation studies (**Figure 3B**). In order to have the same corresponding precursor ion, the tri-ammoniated adduct ($[M–H+3NH_4]^{2+}$) was also chosen for MTX. The measured ion species were assigned for both MTX and MTX4 (**Tables 3** and **4**). The comparison of HRMS/MS spectra in the *m/z* region from 1490 to 1720 led to the identification of $[M–2(SO_3)+2H]^{2+}$ and $[M–2(SO_3)–n(H_2O)+2H]^{2+}$ patterns (**Figures 4A** and **4B**; **Table 3**).

HRMS/MS data in positive ion mode from the present study confirm the presence of two sulfate ester groups in MTX4 and add important information, as they clearly show that MTX4 presents two sulfate losses, in a similar fashion to MTX.

Assignment of MTX product ions

For MTX, the product ions observed at *m/z* 911.5878, 893.5724, 875.5658 and 857.5542 were respectively assigned to the following ion species: $[C_{53}H_{83}O_{12}]^+$, $[C_{53}H_{83}O_{12}–(H_2O)]^+$, $[C_{53}H_{83}O_{12}–2(H_2O)]^+$ and $[C_{53}H_{83}O_{12}–3(H_2O)]^+$ (**Figure 4C**; **Table 4**). Knowledge of the molecular structure of MTX and the elemental formulae of these ions allowed us to attribute these ions to the A-side of the molecule, corresponding to the cleavage **#1** (**Figure 5**).

Indeed, the interpretation of the HRMS/MS fragment ions is in accordance with: (i) the breaking of the $C_{99}–C_{100}$ bond probably associated with ring-opening of ring W at C_{100}-C_{101}, with the positive charge attributed to the A-side, and (ii) subsequent losses of up to three molecules of water (**Figure 5**; **Table 4**).

The cleavage between C_{99} and C_{100} also results in a number of product ions on the right hand side (B-side) of the molecule. On the B-side of the molecule, all the observed product ions appear to have been derived after losses of two sulfates. Fragmentation **#1** (**Figure 5**) was confirmed by the following ions observed at *m/z* 2256.0787, 2238.0846, 2220.0535 and 2202.0443, corresponding to the right hand side (B-side) of the molecule, being assigned to the following ion species: $[C_{111}H_{175}O_{55}S_2–2(SO_3)–n(H_2O)]^+$, where n is respectively equal to 2 to 5 (**Table 4**; **Figure S1, supporting information**). Since the A-side of the molecule had the same elemental formula as the A-side of MTX (structure known, see Figure 5), the elemental formulae proposed for the B-side matched with a high accuracy to the MTX B-side product ions with seven carbons and 17 hydrogens less (while with the other suggested molecular

formula #07, the accuracies for B-side product ions were over 5 ppm). This further corroborates the proposed elemental formula of MTX4.

In addition, the ion at *m/z* 453.2691 (**Table 4**; **Figure S2, supporting information**) was assigned to the elemental formula $C_{21}H_{41}O_{10}^+$. This formula allowed us to correlate this ion to a fragmentation pathway on the central part of the backbone of MTX, i.e. a combination of two cleavages, at **#2**+**#6**, with the opening of the P-ring (**Figure 5**). In analogy, other ions presenting lower *m/z* values could be related to cleavages on the central part of the backbone: (i) the ions at *m/z* 395.2265 and 359.2061 ($C_{18}H_{35}O_9^+$ and $C_{18}H_{31}O_7^+$), resulting from cleavages **#3**+**#6** (**Figure 5**), followed, or not, by two water losses; (ii) the ions at *m/z* 337.1848 and 301.1638 ($C_{15}H_{29}O_8^+$ and $C_{15}H_{25}O_6^+$), resulting from cleavages **#4**+**#6** (**Figure 5**), followed, or not, by two water losses; and (iii) the ion at *m/z* 243.1231 ($C_{12}H_{19}O_5^+$), resulting from cleavages **#4**+**#5** (**Figure 5**) followed by two water losses (**Table 4**; **Figure S2, supporting information**).

Ultimately, the ions at *m/z* 267.1948 and 249.1847 were assigned to ions with elemental formulae of, respectively, $C_{16}H_{27}O_3^+$ and $C_{16}H_{25}O_2^+$. These ions were correlated to a fragmentation pathway on the right side of the molecule, i.e. cleavage **#7** (**Figure 5**), followed by one and two water losses, respectively (**Table 4**; **Figure S2, supporting information**).

All these fragmentations occurred on the B-side tail of MTX backbone and give additional information on the fragmentation pattern of MTX.

Comparison of MTX4 product ions with those of MTX

MTX and MTX4 showed identical product ions in the *m/z* region of 850–920 (**Figures 4C** and **4D**; **Table 4**) corresponding to the left hand side (A-side) of the MTX backbone (cleavage **#1**, **Figure 5**). Probably, as the accurate mass of the A-side product ion is the same in MTX4 as in MTX, this part of the molecule is identical for both MTX and MTX4. Interestingly, some of the lower mass product ions of MTX4 matched with a central part (between cleavages **#2** and **#6**, **Figure 5; Figure S2, supporting information**; **Table 4**) and with the terminal part of the MTX backbone (cleavage **#7**, **Figure 5; Figure S2, supporting information**; **Table 4**), suggesting that these parts of the structure are also conserved between the two molecules. However, no product ions could be assigned to (i) the central part of MTX and MTX4, between cleavages **#1** and **#2** (**Figure 5**), nor to (ii) the right hand side of MTX and MTX4, starting from cleavages **#6** to **#7** (**Figure 5**). Consequently, the nitrogen atom contained in MTX4 should be located in one of these two unresolved parts of the molecule.

CONCLUSIONS

The LC/HRMS and LC-UV analyses of partially purified *G. excentricus* (VGO792) extract carried out in this study provide us more information to clarify the elemental formula of MTX4. First of all, the bathochromic effect of +43 nm compared with MTX and the earlier elution of MTX4 before MTX under acidic conditions, suggested the presence of an amine group situated on a conjugated diene function in MTX4.

Furthermore, the similarities between the ion cluster profiles of the most abundant doubly charged ions of full scan positive and negative MS spectra of MTX and MTX4, allowed us to propose the elemental formula of MTX4 ($C_{157}H_{241}NO_{68}S_2$, as unsalted molecule).

Further investigations of HRMS/MS spectra in positive ion mode were carried out to clarify the fragmentation pathways of MTX and MTX4. Relevant information was provided by the cleavage observed at C_{99}–C_{100} in both MTX and MTX4, highlighting that the same A-side structure is shared by the two molecules. The proposed formula is thus also corroborated by the accuracy of both A- and B-side fproduct ions.

These investigations also confirm that MTX4 belongs to the same structural family of MTXs as MTX. However, in order to accomplish a complete structural elucidation of MTX4, studies based on NMR, LC/HRMS^n, and possibly chemical reactions may have to be carried out [48]. At this stage, we have accumulated a large amount of *G. excentricus* biomass to continue with the isolation of the compound which needs to precede further analytical studies.

ACKNOWLEDGMENTS

The authors would like to acknowledge the provision of strain VGO792 by Santiago Fraga (Instituto Español de Oceanografía, Vigo, Spain), which had been cultivated at Ifremer in 2017 and is now no longer in culture at Ifremer. The authors acknowledge Ifremer and the Regional Council of the *Région des Pays de la Loire* for PhD funding of FP (up to 30/09/2017). MS and PH acknowledge funding from the European Union through Interreg AlertoxNet EAPA-317-2016.

AUTHORS' CONTRIBUTION

FP, MS, PH and CH conceived the study. FP and RW conducted experimental work on purification of MTX4. FP and CH performed the LC-UV analysis. FP, MS and RW performed the chemical analysis on LC-HRMS/MS. FP, MS, CR, PH and CH contributed to writing the manuscript. FP, MS, CR, RW, TS, PH and CH reviewed the manuscript. TS and PH were involved in obtaining funding for this research.

REFERENCES

1. Friedman MA, Fernandez M, Backer LC, et al. An updated review of ciguatera fish poisoning: Clinical, epidemiological, environmental, and public health management. *Mar Drugs*. 2017;15(3). doi:10.3390/md15030072
2. Soliño L, Costa PR. Global impact of ciguatoxins and ciguatera fish poisoning on fish, fisheries and consumers. *Environ Res*. 2020;182. doi:10.1016/j.envres.2020.109111
3. Tester PA, Litaker RW, Berdalet E. Climate change and harmful benthic microalgae. *Harmful Algae*. 2019. doi:10.1016/j.hal.2019.101655
4. Fraga S, Rodríguez F, Caillaud A, Diogène J, Raho N, Zapata M. *Gambierdiscus excentricus* sp. nov. (Dinophyceae), a benthic toxic dinoflagellate from the Canary Islands (NE Atlantic Ocean). *Harmful Algae*. 2011;11:10-22. doi:10.1016/j.hal.2011.06.013
5. Litaker RW, Holland WC, Hardison DR, et al. Ciguatoxicity of *Gambierdiscus* and *Fukuyoa* species from the Caribbean and Gulf of Mexico. *PLoS One*. 2017;12(10). doi:10.1371/journal.pone.0185776
6. Pisapia F, Holland WC, Hardison DR, et al. Toxicity screening of 13 *Gambierdiscus* strains using neuro-2a and erythrocyte lysis bioassays. *Harmful Algae*. 2017;63. doi:10.1016/j.hal.2017.02.005
7. Rossignoli AE, Tudó A, Bravo I, Díaz PA, Diogène J, Riobó P. Toxicity characterisation of *Gambierdiscus* species from the Canary Islands. *Toxins (Basel)*. 2020;12(2):134. doi:10.3390/toxins12020134
8. Shmukler YB, Nikishin DA. Ladder-shaped ion channel ligands: Current state of knowledge. *Mar Drugs*. 2017. doi:10.3390/md15070232
9. Munday R. Toxicology of Seafood Toxins: A Critical Review. In: *Seafood and Freshwater Toxins*. ; 2014. doi:10.1201/b16662-7
10. Murata M, Sasaki M, Yokoyama A, et al. Structure of maitotoxin. *J Am Chem Soc*. 1993;115(5):2060-2062. doi:10.1021/ja00058a075
11. Kohli GS, Papiol GG, Rhodes LL, et al. A feeding study to probe the uptake of maitotoxin by snapper (*Pagrus auratus*). *Harmful Algae*. 2014;37(0):125-132. doi:10.1016/j.hal.2014.05.018
12. Yasumoto T, Bagnis R, Vernoux JP. Toxicity of the surgeonfishes II. Properties of the principal water-soluble toxin. *Nippon Suisan Gakkaishi*. 1976. doi:10.2331/suisan.42.359
13. Yasumoto T, Hashimoto Y, Bagnis R, Randall JE, Banner AH. Toxicity of the surgeonfishes. *Bull Jap Soc Sci Fish*. 1971;37(8):724-734.
14. Yasumoto T, Seino N, Murakami Y, Murata M. Toxins produced by benthic dinoflagellates. *Biol Bull*. 1987;172(1):128-131. doi:10.2307/1541612
15. Holmes MJ, Lewis RJ, Gillespie NC. Toxicity of Australian and French Polynesian strains of

Gambierdiscus toxicus (Dinophyceae) grown in culture: Characterization of a new type of maitotoxin. *Toxicon*. 1990;28(10):1159-1172. doi:10.1016/0041-0101(90)90116-O

16. Holmes MJ, Lewis RJ. Purification and characterisation of large and small maitotoxins from cultured *Gambierdiscus toxicus*. *Nat Toxins*. 1994;2(2):64-72. doi:10.1002/nt.2620020204
17. Pisapia F, Sibat M, Herrenknecht C, et al. Maitotoxin-4, a novel MTX analog produced by *Gambierdiscus excentricus*. *Mar Drugs*. 2017;15(7). doi:10.3390/md15070220
18. Mazzola EP, Deeds JR, Stutts WL, et al. Elucidation and partial NMR assignment of monosulfated maitotoxins from the Caribbean. *Toxicon*. 2019;164:44-50. doi:10.1016/j.toxicon.2019.03.026
19. Sasaki M, Murata M. Complete structure of maitotoxin. *J Synth Org Chem Japan*. 1997;55(6):535-546.
20. Nonomura T, Sasaki M, Matsumori N, Murata M, Tachibana K, Yasumoto T. The complete structure of maitotoxin. 2. Configuration of the C_{135}-C_{142} side chain and absolute configuration of the entire molecule. *Angew Chemie-International Ed English*. 1996;35(15):1675-1678. doi:10.1002/anie.199616751
21. Rhodes LL, Smith KF, Murray S, Harwood DT, Trnski T, Munday R. The epiphytic genus *Gambierdiscus* (Dinophyceae) in the Kermadec Islands and Zealandia regions of the southwestern Pacific and the associated risk of ciguatera fish poisoning. *Mar Drugs*. 2017;15(7). doi:10.3390/md15070219
22. Rhodes LL, Smith KF, Verma A, Murray S, Harwood DT, Trnski T. The dinoflagellate genera *Gambierdiscus* and *Ostreopsis* from subtropical Raoul Island and North Meyer Island, Kermadec Islands. *New Zeal J Mar Freshw Res*. 2017;51(4):490-504. doi:10.1080/00288330.2016.1270337
23. Munday R, Murray S, Rhodes LL, Larsson ME, Harwood DT. Ciguatoxins and maitotoxins in extracts of sixteen *Gambierdiscus* isolates and one *Fukuyoa* isolate from the South Pacific and their toxicity to mice by intraperitoneal and oral administration. *Mar Drugs*. 2017;15(7). doi:10.3390/md15070208
24. Rhodes LL, Harwood DT, Smith KF, Argyle P, Munday R. Production of ciguatoxin and maitotoxin by strains of *Gambierdiscus australes*, *G. pacificus* and *G. polynesiensis* (Dinophyceae) isolated from Rarotonga, Cook Islands. *Harmful Algae*. 2014;39(0):185-190. doi:10.1016/j.hal.2014.07.018
25. Rhodes LL, Papiol GG, Smith KF, Harwood DT. *Gambierdiscus* cf. *yasumotoi* (Dinophyceae) isolated from New Zealand's sub-tropical northern coastal waters. *New Zeal J Mar Freshw Res*. 2014;48(2):303-310. doi:10.1080/00288330.2013.870220
26. Rhodes LL, Harwood DT, Smith KF, Argyle P, Munday R. Corrigendum to 'Production of ciguatoxin and maitotoxin by strains of *Gambierdiscus australes*, *G. pacificus* and *G. polynesiensis* (Dinophyceae) isolated from Rarotonga, Cook Islands' [Harmful Algae 39 (2014)

185–190] (S1568988314001449. *Harmful Algae*. 2016. doi:10.1016/j.hal.2016.03.014

27. Kohli G. Diversity and genetics of Australasian dinoflagellates, including *Gambierdiscus* spp. the causative agent of ciguatera fish poisoning. PhD thesis. 2014. http://handle.unsw.edu.au/1959.4/53428.
28. Pisapia F. Bioguided screening and LC-HRMS for identification of toxins and other metabolites of interest produced by the dinoflagellates *Gambierdiscus* and *Fukuyoa*. PhD thesis. 2017. https://www.theses.fr/2017NANT4056.pdf.
29. Smith KF, Rhodes LL, Verma A, et al. A new *Gambierdiscus* species (Dinophyceae) from Rarotonga, Cook Islands: *Gambierdiscus cheloniae* sp. nov. *Harmful Algae*. 2016. doi:10.1016/j.hal.2016.10.006
30. Rhodes LL, Smith KF, Verma A, et al. A new species of *Gambierdiscus* (Dinophyceae) from the south-west Pacific: *Gambierdiscus honu* sp. nov. *Harmful Algae*. 2017. doi:10.1016/j.hal.2017.04.010
31. Kretzschmar AL, Verma A, Harwood DT, Hoppenrath M, Murray SA. Characterization of *Gambierdiscus lapillus* sp. nov. (Gonyaulacales, Dinophyceae): a new toxic dinoflagellate from the Great Barrier Reef (Australia). DeClerck O, ed. *J Phycol*. 2017;53(2):283-297. doi:10.1111/jpy.12496
32. Larsson ME, Harwood DT, Lewis RJ, Himaya SWA, Doblin MA. Toxicological characterization of *Fukuyoa paulensis* (Dinophyceae) from temperate Australia. *Phycol Res*. 2019. doi:10.1111/pre.12349
33. Murray JS, Boundy MJ, Selwood AI, Harwood DT. Development of an LC–MS/MS method to simultaneously monitor maitotoxins and selected ciguatoxins in algal cultures and P-CTX-1B in fish. *Harmful Algae*. 2018;80:80-87. doi:10.1016/j.hal.2018.09.001
34. Larsson ME, Laczka OF, Harwood DT, et al. Toxicology of *Gambierdiscus* spp. (Dinophyceae) from tropical and temperate Australian waters. *Mar Drugs*. 2018;16(1). doi:10.3390/md16010007
35. Leung PTY, Yan M, Lam VTT, et al. Phylogeny, morphology and toxicity of benthic dinoflagellates of the genus *Fukuyoa* (Goniodomataceae, Dinophyceae) from a subtropical reef ecosystem in the South China Sea. *Harmful Algae*. 2018;74:78-97. doi:10.1016/j.hal.2018.03.003
36. Argyle PA, Harwood DT, Rhodes LL, Champeau O, Tremblay LA. Toxicity assessment of New Zealand and Pacific dinoflagellates *Ostreopsis* and *Gambierdiscus* (Dinophyceae) extracts using bioassays. *New Zeal J Mar Freshw Res*. 2016;50(3). doi:10.1080/00288330.2016.1159581
37. Larsson ME. Toxicology and ecology of *Gambierdiscus* from Australia: a dinoflagellate genus associated with ciguatera fish poisoning. PhD thesis. 2019. http://hdl.handle.net/10453/133326.
38. Murray JS, Selwood AI, Harwood DT, et al. 44-methylgambierone, a new gambierone analogue isolated from *Gambierdiscus australes*. *Tetrahedron Lett*. 2019;60(8):621-625.

doi:10.1016/j.tetlet.2019.01.043

39. Boente-Juncal A, Álvarez M, Antelo Á, et al. Structure elucidation and biological evaluation of maitotoxin-3, a homologue of gambierone, from *Gambierdiscus belizeanus*. *Toxins (Basel)*. 2019;11(2):79. doi:10.3390/toxins11020079
40. Rodríguez I, Genta-Jouve G, Alfonso C, et al. Gambierone, a ladder-shaped polyether from the dinoflagellate *Gambierdiscus belizeanus*. *Org Lett*. 2015;17(10):2392-2395. doi:10.1021/acs.orglett.5b00902
41. Longo S, Sibat M, Viallon J, Darius HT, Hess P, Chinain M. Intraspecific variability in the toxin production and toxin profiles of in vitro cultures of *Gambierdiscus polynesiensis* (Dinophyceae) from French polynesia. *Toxins (Basel)*. 2019;11(12):1-23. doi:10.3390/toxins11120735
42. Kretzschmar AL, Larsson ME, Hoppenrath M, Doblin MA, Murray SA. Characterisation of two toxic *Gambierdiscus* spp. (Gonyaulacales, Dinophyceae) from the Great Barrier Reef (Australia): *G. lewisii* sp. nov. and *G. holmesii* sp. nov. *Protist*. 2019;170(6):125699. doi:10.1016/j.protis.2019.125699
43. Lewis RJ, Holmes MJ, Alewood PF, Jones A. Ionspray mass spectrometry of ciguatoxin-1, maitotoxin-2 and -3, and related marine polyether toxins. *Nat Toxins*. 1994;2(2):56-63. doi:10.1002/nt.2620020203
44. Patiny L, Borel A. ChemCalc: A building block for tomorrow's chemical infrastructure. *J Chem Inf Model*. 2013. doi:10.1021/ci300563h
45. Yokoyama A, Murata M, Oshima Y, Iwashita T, Yasumoto T. Some chemical properties of maitotoxin, a putative calcium channel agonist isolated from a marine dinoflagellate. *J Biochem*. 1988;104(2):184-187. doi:10.1093/oxfordjournals.jbchem.a122438
46. Cranwell PB, Harwood LM, Moody CJ. *Experimental Organic Chemistry, Third Edition*. Wiley; 2017.
47. McLafferty FW, Turecek F. *Interpretation of Mass Spectra*. Sausalito, California (USA): University Science Books; 1993.
48. Satake M, Yasumoto T. Methods for determining the absolute configurations of marine ladder-shaped polyethers. *Chirality*. 2020. doi:10.1002/chir.23187

Table 1. Comparison of retention times (*RT*, min) in UPLC/HRMS analysis of maitotoxin (MTX) and maitotoxin-4 (MTX4) between this study and Pisapia et al [17]. The two studies used the same chromatographic conditions except for the composition of the mobile phases.

Ref.	**Mobile phases**	**Retention time** (*RT*, min)		**Ionisation mode**
	A: H_2O **B: MeCN:H_2O (95:5, *v/v*)**	**MTX**	**MTX4**	
Pisapia, et al. [13]	**Without acidic buffer**	4.09	4.58	NEG
This study	**With acidic buffer ***	5.74	5.56	POS

* formic acid (HCOOH, 50 mM) and ammonium formate ($HCOO^-NH_4^+$, 2 mM)

Table 2. List of the assigned HRMS ion species for MTX and MTX4 in positive and in negative ESI ionization modes. The *m/z* values in the Table correspond to the accurate mono-isotopic ion *m/z*. Mass differences (Δppm) for MTX and MTX4 were compared between measured and exact theoretical mass.

		MTX (*m/z*)	**MTX4 (*m/z*)**	**Ref.**
Elemental formula (free acid form)		$C_{164}H_{258}O_{68}S_2$	$C_{157}H_{241}NO_{68}S_2$	
Ion species (accurate mono-isotopic)	$[M+2H]^{2+}$	1690.8166 (Δppm: +0.4)	1647.2500 (Δppm: −0.5)	This study
	$[M+H+NH_4]^{2+}$	1699.3240 (Δppm: –3.0)	1655.7575 (Δppm: −4.0)	This study
	$[M+2NH_4]^{2+}$	1707.8323 (Δppm: –5.9)	1664.2725 (Δppm: −3.0)	This study
	$[M-H+3NH_4]^{2+}$	1716.3500 (Δppm: –3.3)	1672.7870 (Δppm: −2.2)	This study
	$[M-2H]^{2-}$	1688.8027 (Δppm: +0.8)	1645.2357 (Δppm: −0.4)	Pisapia et al [17]
	$[M+Na-3H]^{2-}$	1699.7914 (Δppm: –0.5)	1656.2256 (Δppm: −1.0)	Pisapia et al [17]
	$[M+2Na-4H]^{2-}$	1710.7814 (Δppm: –1.1)	1667.2075 (Δppm: −6.5)	Pisapia et al [17]
	$[M-3H]^{3-}$	1125.5334 (Δppm: +1.4)	1096.4889 (Δppm: +0.4)	Pisapia et al [17]
	$[M-4H]^{4-}$	843.8989 (Δppm: +2.3)	n.d*	Pisapia et al [17]

*n.d: non detected

Table 3. List of the assigned HRMS/MS ion species deriving from losses of H_2O and SO_3 for MTX and MTX4 (other ion species corresponding to product ions suggested in Figure 5 are reported in Table 4). Accurate mass data were obtained from HRMS/MS spectra of $[M–H+3NH_4]^{2+}$ with a collision energy (CE) of 40 eV for MTX and MTX4. The *m/z* values in the Table correspond to the accurate mono-isotopic *m/z*.

	Ion species	MTX				MTX4			
		Elemental formula	**Theoretical *m/z***	**Experimental *m/z***	**Δppm**	**Elemental formula**	**Theoretical *m/z***	**Experimental *m/z***	**Δppm**
Parent ion	$[M–H+3NH_4]^{2+}$	$C_{164}H_{269}N_3O_{68}S_2^{(2+)}$	1716.3557	1716.3500	–3.3	$C_{157}H_{252}N_4O_{68}S_2^{(2+)}$	1672.7907	1672.7870	–2.2
Fragment ions	$[M–(SO_3)+2H]^{2+}$	$C_{164}H_{260}O_{65}S^{(2+)}$	1650.8375	1650.8388	+0.8	$C_{157}H_{243}NO_{65}S^{(2+)}$	1607.2725	1607.2672	–3.3
	$[M–(SO_3)–1(H_2O)+2H]^{2+}$	$C_{164}H_{258}O_{64}S^{(2+)}$	1641.8322	1641.8229	–5.7	$C_{157}H_{241}NO_{64}S^{(2+)}$	1598.2672	1598.2636	–2.3
	$[M–(SO_3)–2(H_2O)+2H]^{2+}$	$C_{164}H_{256}O_{63}S^{(2+)}$	1632.8269	1632.8155	–7.0	$C_{157}H_{239}NO_{63}S^{(2+)}$	1589.2619	1589.2489	–8.2
	$[M–(SO_3)–3(H_2O)+2H]^{2+}$	$C_{164}H_{254}O_{62}S^{(2+)}$	1623.8216	1623.8072	–8.9	$C_{157}H_{237}NO_{62}S^{(2+)}$	1580.2566	1580.2407	–10.1
	$[M–(SO_3)–4(H_2O)+2H]^{2+}$	$C_{164}H_{252}O_{61}S^{(2+)}$	1614.8163	n.d*		$C_{157}H_{235}NO_{61}S^{(2+)}$	1571.2514	1571.2466	–3.1
	$[M–2(SO_3)+2H]^{2+}$	$C_{164}H_{260}O_{62}^{(2+)}$	1610.8591	1610.8500	–5.6	$C_{157}H_{243}NO_{62}^{(2+)}$	1567.2941	n.d	
	$[M–2(SO_3)–1(H_2O)+2H]^{2+}$	$C_{164}H_{258}O_{61}^{(2+)}$	1601.8538	1601.8365	–10.8	$C_{157}H_{241}NO_{61}^{(2+)}$	1558.2888	1558.2819	–4.4
	$[M–2(SO_3)–2(H_2O)+2H]^{2+}$	$C_{164}H_{256}O_{60}^{(2+)}$	1592.8485	1592.8335	–9.4	$C_{157}H_{239}NO_{60}^{(2+)}$	1549.2835	1549.2723	–7.2
	$[M–2(SO_3)–3(H_2O)+2H]^{2+}$	$C_{164}H_{254}O_{59}^{(2+)}$	1583.8432	1583.8317	–7.3	$C_{157}H_{237}NO_{59}^{(2+)}$	1540.2782	1540.2789	+0.5
	$[M–2(SO_3)–4(H_2O)+2H]^{2+}$	$C_{164}H_{252}O_{58}^{(2+)}$	1574.8379	1574.8227	–9.7	$C_{157}H_{235}NO_{58}^{(2+)}$	1531.2729	1531.2603	–8.2
	$[M–2(SO_3)–5(H_2O)+2H]^{2+}$	$C_{164}H_{250}O_{57}^{(2+)}$	1565.8327	1565.8163	–10.5	$C_{157}H_{233}NO_{57}^{(2+)}$	1522.2677	1522.2777	+6.6
	$[M–2(SO_3)–6(H_2O)+2H]^{2+}$	$C_{164}H_{248}O_{56}^{(2+)}$	1556.8274	1556.8155	–7.6	$C_{157}H_{231}NO_{56}^{(2+)}$	1513.2624	1513.2920	+19.6
	$[M–2(SO_3)–7(H_2O)+2H]^{2+}$	$C_{164}H_{246}O_{55}^{(2+)}$	1547.8221	1547.8135	–5.6	$C_{157}H_{229}NO_{55}^{(2+)}$	1504.2571	1504.2389	–12.1
	$[M–2(SO_3)–8(H_2O)+2H]^{2+}$	$C_{164}H_{244}O_{54}^{(2+)}$	1538.8168	1538.8164	–0.3	$C_{157}H_{227}NO_{54}^{(2+)}$	1495.2518	1495.2651	+8.9

*n.d: non detected

Table 4. Assignment of HRMS/MS product ions observed in HR CID MS² spectra of MTX and MTX4, corresponding to the cleavages reported in **Figure 5**. Accurate measured mass data were obtained from HRMS/MS spectra of $[M–H+3NH_4]^{2+}$ with three fixed collision energies (CE = 30, 40 and 50 eV) for both molecules. The *m/z* values in the Table correspond to the accurate mono-isotopic *m/z*.

Cleavage	MTX						MTX4					
	Theoretical *m/z*	Experimental *m/z*	Water losses	Formula[a]	RDB[b]	Δppm[c]	Theoretical *m/z*	Experimental *m/z*	Water losses	Formula	RDB	Δppm
#1/ A-side	911.5879	911.5878		$C_{53}H_{83}O_{12}^+$	12	–0.1	911.5879	911.5877		$C_{53}H_{83}O_{12}^+$	12	–0.2
	893.5773	893.5724	1	$C_{53}H_{81}O_{11}^+$	13	–5.5	893.5773	893.5758	1	$C_{53}H_{81}O_{11}^+$	13	–1.7
	875.5668	875.5658	2	$C_{53}H_{79}O_{10}^+$	14	–1.1	875.5668	875.5644	2	$C_{53}H_{79}O_{10}^+$	14	–2.7
	857.5562	857.5542	3	$C_{53}H_{77}O_9^+$	15	–2.3	857.5562	857.5556	3	$C_{53}H_{77}O_9^+$	15	–0.7
#1/ B-side	2256.0985	2256.0787	2	$C_{111}H_{171}O_{47}^+$	26	–8.8	2168.9686	2168.9692	2	$C_{104}H_{154}NO_{47}^+$	28	+0.3
	2238.0879	2238.0846	3	$C_{111}H_{169}O_{46}^+$	27	–1.5	2150.9580	2150.9541	3	$C_{104}H_{152}NO_{46}^+$	29	–1.8
	2220.0774	2220.0535	4	$C_{111}H_{167}O_{45}^+$	28	–10.8	2132.9474	2132.9391	4	$C_{104}H_{150}NO_{45}^+$	30	–3.9
	2202.0668	2202.0443	5	$C_{111}H_{165}O_{44}^+$	29	–10.2	2114.9369	2114.9360	5	$C_{104}H_{148}NO_{44}^+$	31	–0.4
#2+**#6**	453.2694	453.2691		$C_{21}H_{41}O_{10}^+$	1	–0.7	453.2694	453.2681		$C_{21}H_{41}O_{10}^+$	1	–2.9
#2+**#6**–$2H_2O$	417.2483	n.d[d]	2	$C_{21}H_{37}O_8^+$			417.2483	417.2475	2	$C_{21}H_{37}O_8^+$	3	–1.9
#3+**#6**	395.2276	395.2265		$C_{18}H_{35}O_9^+$	1	–2.8	395.2276	395.2265		$C_{18}H_{35}O_9^+$	1	–2.8
#3+**#6**–$2H_2O$	359.2064	359.2061	2	$C_{18}H_{31}O_7^+$	3	–0.8	359.2064	359.2053	2	$C_{18}H_{31}O_7^+$	3	–3.1
#4+**#6**	337.1857	337.1848		$C_{15}H_{29}O_8^+$	1	–2.7	337.1857	337.1846		$C_{15}H_{29}O_8^+$	1	–3.3
#4+**#6**–$2H_2O$	301.1646	301.1638	2	$C_{15}H_{25}O_6^+$	3	–2.7	301.1646	301.1644	2	$C_{15}H_{25}O_6^+$	3	–0.7
#4+**#5**–$2H_2O$	243.1227	243.1231	2	$C_{12}H_{19}O_5^+$	3	+1.6	243.1227	243.1226	2	$C_{12}H_{19}O_5^+$	3	–0.4
#7–H_2O	267.1955	267.1948	1	$C_{16}H_{27}O_3^+$	3	–2.6	267.1955	267.1952	1	$C_{16}H_{27}O_3^+$	3	–1.1
#7–$2H_2O$	249.1849	249.1847	2	$C_{16}H_{25}O_2^+$	4	–0.8	249.1849	249.1861	2	$C_{16}H_{25}O_2^+$	4	+4.8

[a]: Elemental formula
[b]: Relative Double Bond equivalent
[c]: Error in ppm
[d]: non detected

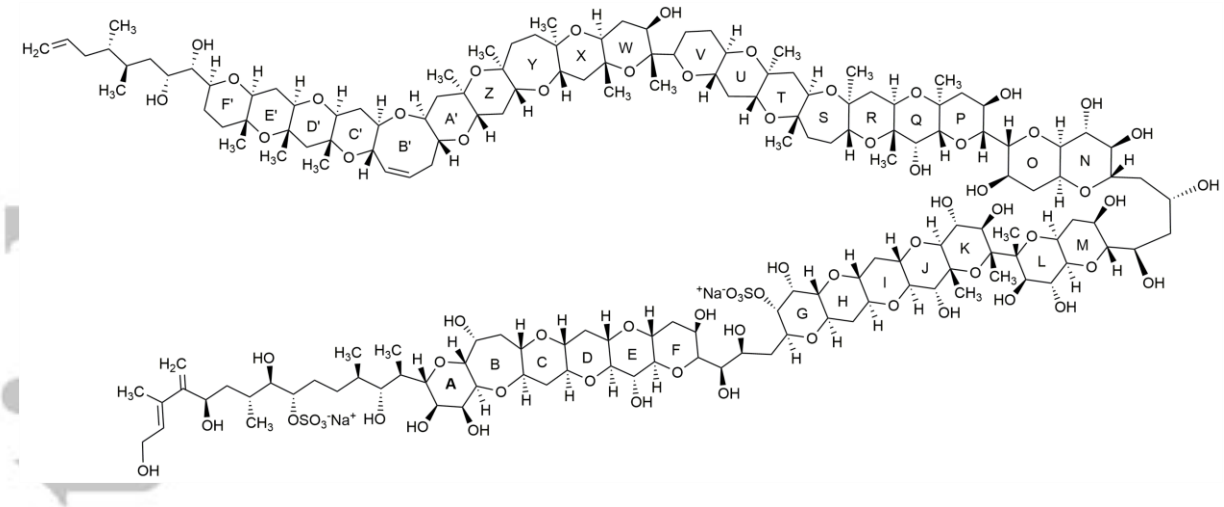

Figure 1. Structure of maitotoxin (MTX) 9 with absolute stereochemistry according to Sasaki, et al 18 and Nonomura, et al 19.

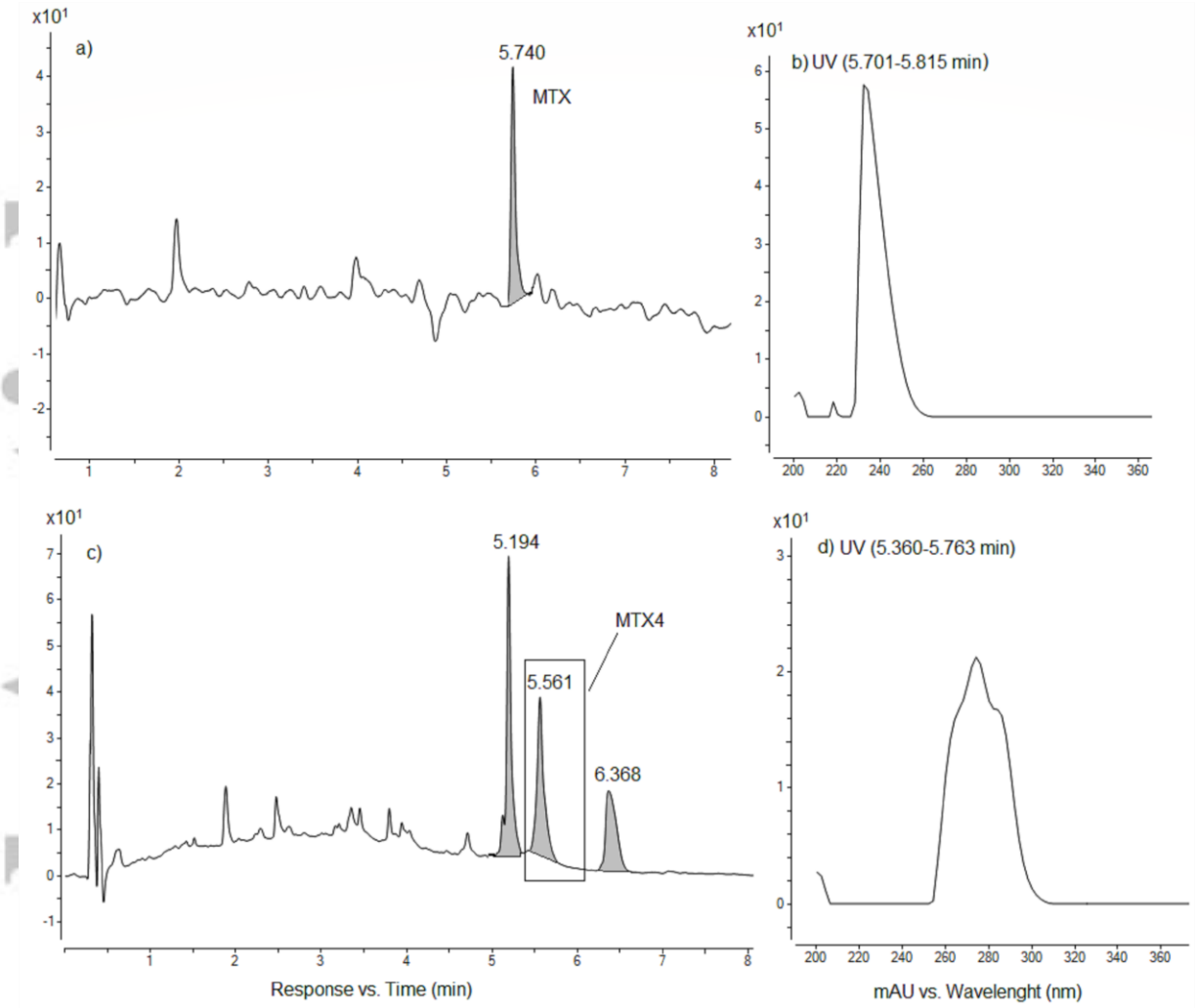

Figure 2. HPLC-UV chromatogram and UV spectra of (A), (B) maitotoxin (MTX) standard (20 μg mL–1) and (C), (D) maitotoxin-4 (MTX4) from G. excentricus VGO792. MTX standard is characterized by a single UV absorbance maximum at λmax = 232 nm. MTX4 has a UV maximum peak at λ = 275 nm between two shoulders.

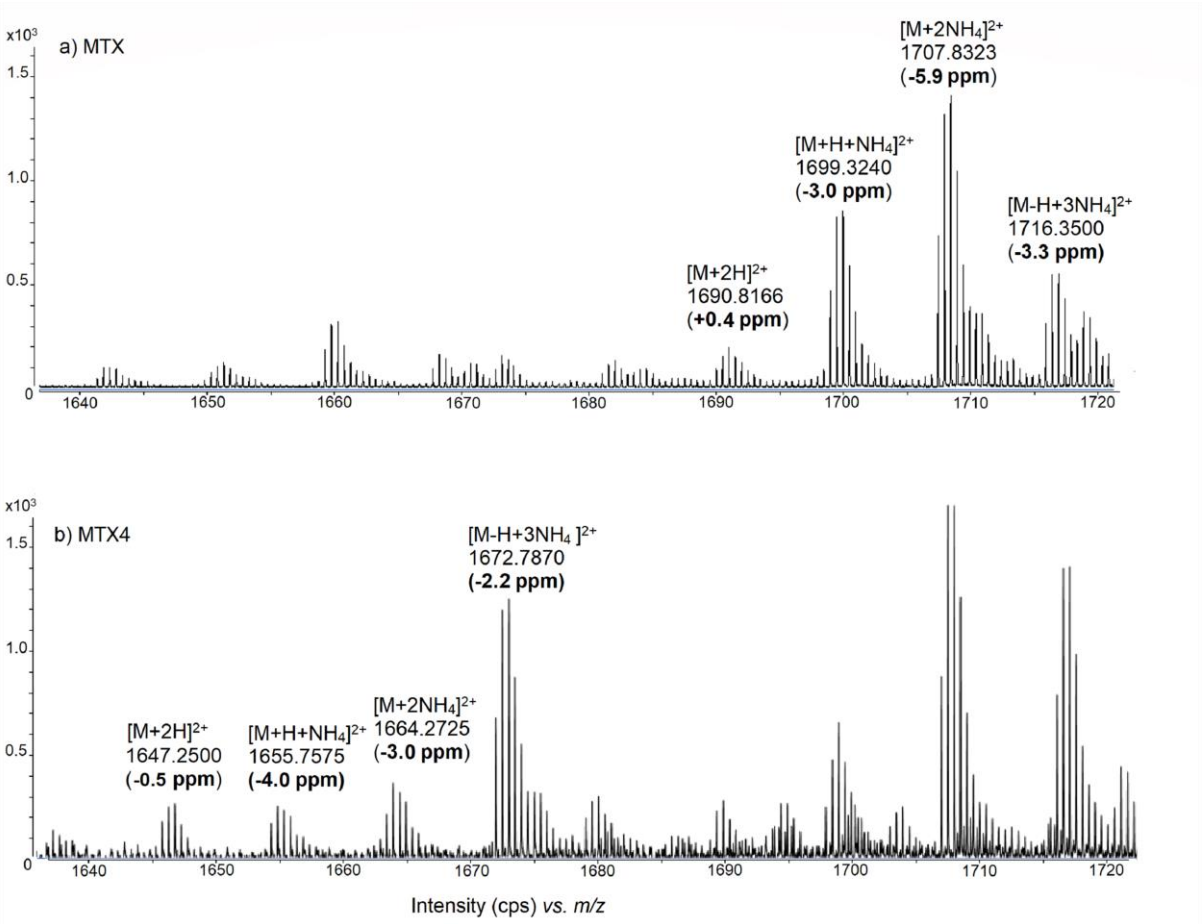

Figure 3. Positive electrospray HRMS spectra of (A) maitotoxin (MTX) standard (Wako, 50 μg mL−1) and (B) maitotoxin-4 (MTX4) from G. excentricus VGO792.

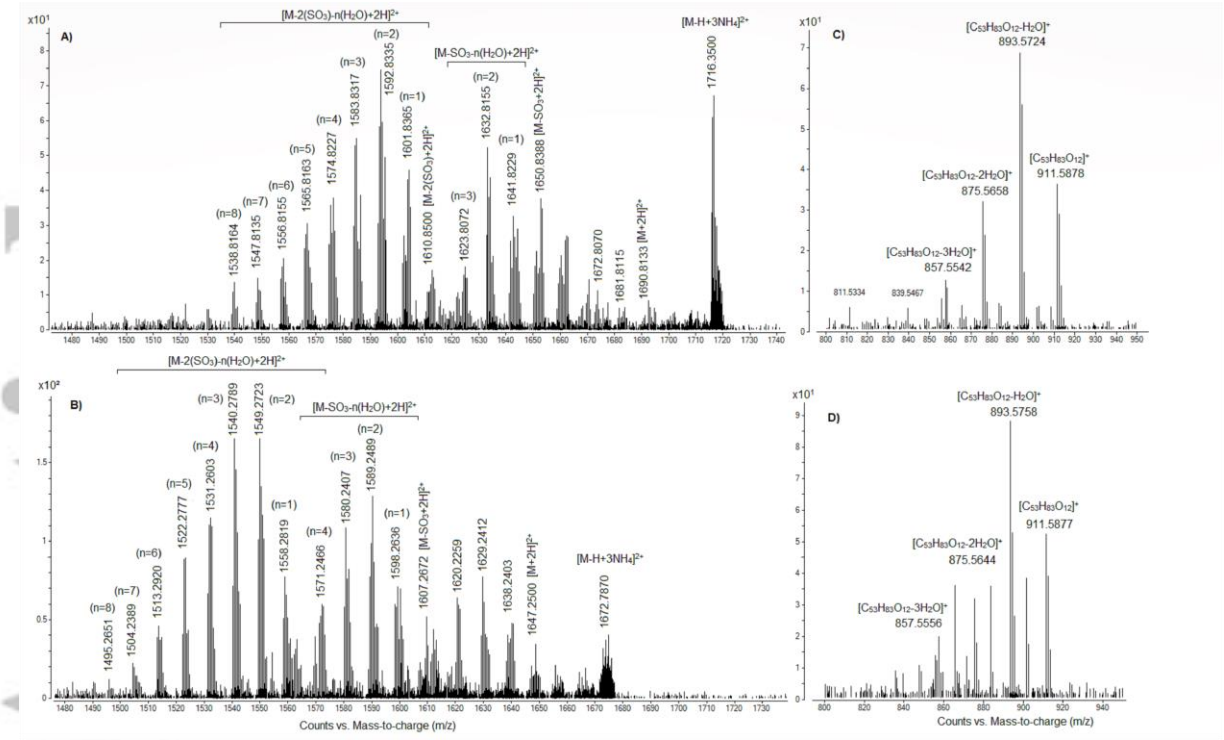

Figure 4. HRMS/MS spectra of (A), (C) maitotoxin (MTX) standard (Wako, 50 μg mL–1) and (B), (D) maitotoxin-4 (MTX4) from G. excentricus VGO792. (A) and (B) focuses on a mass range of 1490–1720 and MS/MS spectra were obtained targeting [M–H+3NH4]2+ with a collision energy (CE) of 40 eV. Note the clusters [M–2(SO3)–n(H2O)+2H]2+. (C) and (D) focuses on a mass range of 846–926 and MS/MS spectra were obtained targeting [M–H+3NH4]2+ with a CE of 50 eV.

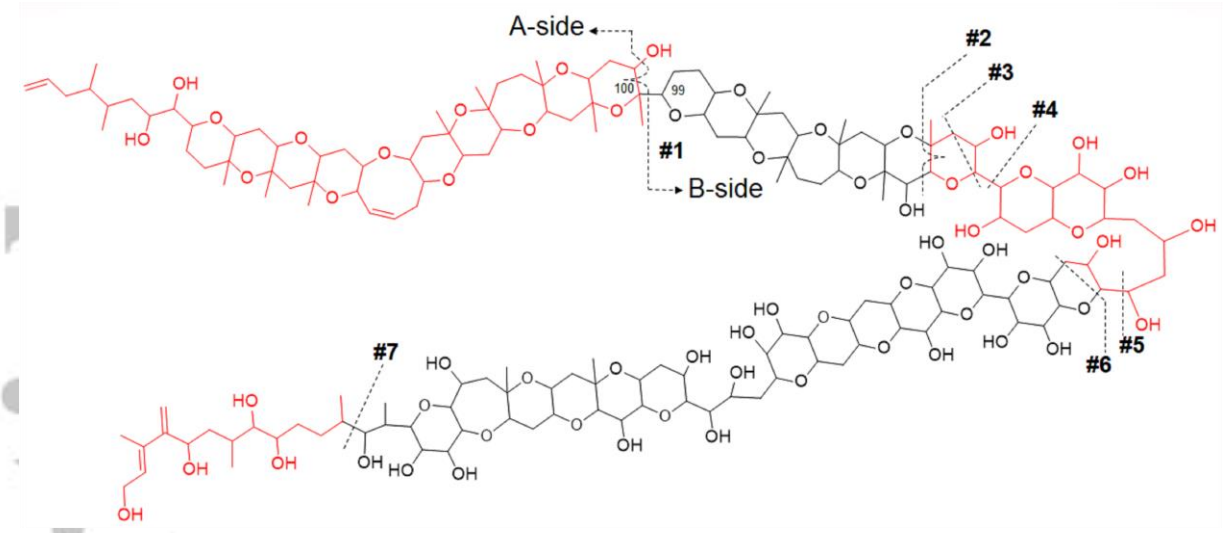

Figure 5. Planar representation of the structure of bis-desulfated maitotoxin (9,40-didesulfoMTX) with the proposed fragmentation cleavages in positive ESI HRMS/MS analysis. The structural parts shared by MTX and MTX4 are highlighted in red. Assignment of fragment ions is reported in Table 4.